MITIGATING BIAS IN CALIBRATION ERROR ESTIMATION

Anonymous authors
Paper under double-blind review

ABSTRACT

Building reliable machine learning systems requires that we correctly understand their level of confidence. Calibration focuses on measuring the degree of accuracy in a model's confidence and most research in calibration focuses on techniques to improve an empirical estimate of calibration error, ECE_{BIN}. Using simulation, we show that ECE_{BIN} can systematically underestimate or overestimate the true calibration error depending on the nature of model miscalibration, the size of the evaluation data set, and the number of bins. Critically, ECE_{BIN} is more strongly biased for perfectly calibrated models. We propose a simple alternative calibration error metric, $\text{ECE}_{\text{SWEEP}}$, in which the number of bins is chosen to be as large as possible while preserving monotonicity in the calibration function. Evaluating our measure on distributions fit to neural network confidence scores on CIFAR-10, CIFAR-100, and ImageNet, we show that $\text{ECE}_{\text{SWEEP}}$ produces a less biased estimator of calibration error and therefore should be used by any researcher wishing to evaluate the calibration of models trained on similar datasets.

1 INTRODUCTION

Machine learning models are increasingly deployed in high-stakes settings like self-driving cars (Caesar et al., 2020; Geiger et al., 2013; Sun et al., 2020) and medical diagnoses (Esteva et al., 2017; 2019; Gulshan et al., 2016) where a model's ability to recognize when it is likely to be incorrect is critical. Unfortunately, such models often fail in unexpected and poorly understood ways, hindering our ability to interpret and trust such systems (Azulay & Weiss, 2018; Biggio & Roli, 2018; Hendrycks & Dietterich, 2019; Recht et al., 2019; Szegedy et al., 2013). To address these issues, calibration is used to ensure that a machine learning model produces confidence scores that reflect the model's ground truth likelihood of being correct (Platt et al., 1999; Zadrozny & Elkan, 2001; 2002).

To obtain an estimate of the calibration error, or ECE[1], the standard procedure (Guo et al., 2017; Naeini et al., 2015) partitions the model confidence scores into bins and compares the model's predicted accuracy to its empirical accuracy within each bin. We refer to this specific metric as ECE_{BIN}. Although recent work has pointed out that ECE_{BIN} is sensitive to implementation hyperparameters (Kumar et al., 2019; Nixon et al., 2019), measuring the statistical bias in ECE_{BIN}, or the difference between the expected ECE_{BIN} and the true calibration error (TCE), has remained largely unaddressed.

In this paper, we address this problem by developing techniques to measure bias in existing calibration metrics. We use simulation to create a setting where the TCE can be computed analytically and thus the bias can be estimated directly. (For a look ahead at the type of assumptions we make, see Figure 1b.) We find empirically that ECE_{BIN} has non-negligible statistical bias and, as Figure 1a highlights, systematically predicts large calibration errors for perfectly calibrated models.

Motivated by monotonicity in true calibration curves arising from trained models, we develop a simple alternate for measuring calibration error, the *monotonic sweep calibration error* ($\text{ECE}_{\text{SWEEP}}$), which chooses the largest number possible while maintaining monotonicity in the approximation to the calibration curve. Our results suggest that $\text{ECE}_{\text{SWEEP}}$ is less biased than the standard ECE_{BIN} and can thus more reliably estimate calibration error.

[1]Naeini et al. (2015) introduce ECE as an acronym for *Expected* Calibration Error. However, ECE is not a proper expectation whereas the true calibration error is computed under an expectation. To resolve this confusion, we prefer to read ECE as *Estimated* Calibration Error.

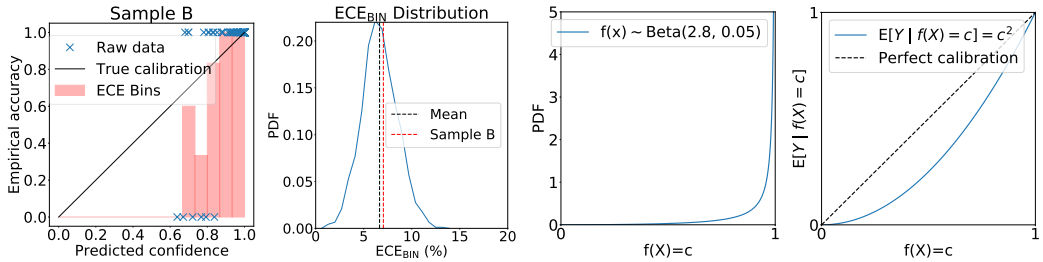

(a) **Bias in ECE_{BIN} for perfectly calibrated models.** (b) **Curves controlling true calibration error.**

Figure 1: 1a: Simulated data from a perfectly calibrated model for a beta distribution fit to CIFAR-10 ResNet-110 data (He et al., 2016; Kängsepp, 2019)). We show a reliability diagram for a single sample of size $n = 200$ and the distribution of ECE_{BIN} scores computed across 10^6 independent simulations. Even though the model is perfectly calibrated (TCE = 0%), ECE_{BIN} systematically predicts large calibration errors (average ECE_{BIN} estimate is 6.8%). 1b: Our ability to measure calibration is contingent on both the confidence score distribution (e.g., $f(X) \sim \text{Beta}(2.8, 0.05)$) and the true calibration curve (e.g., $\mathbb{E}_Y[Y \mid f(X) = c] = c^2$.

2 Theoretical and Empirical Measures of Calibration Error

Suppose we are in a binary classification setup with input $X \in \mathcal{X}$, target output $Y = \{0, 1\}$, and we have a model $f : X \to [0, 1]$ whose output represents a confidence score that the true label Y is 1.

True calibration error (TCE). We define true calibration error as the difference between a model's predicted confidence and the true likelihood of being correct under the ℓ_p norm:

$$\text{TCE}(f) = \left(\mathbb{E}_X\left[|f(X) - \mathbb{E}_Y[Y|f(X)]|^p\right]\right)^{\frac{1}{p}}. \tag{1}$$

The TCE is dictated by two independent features of a model: (1) the distribution of confidence scores $f(x) \sim \mathcal{F}$ over which the outer expectation is computed, and (2) the true calibration curve $\mathbb{E}_Y[Y \mid f(X)]$, which governs the relationship between the confidence score $f(x)$ and the empirical accuracy (Figure 1b). In our experiments, we measure calibration error using the ℓ_2 norm because it increases the sensitivity of the error metric to extremely poorly calibrated predictions, which tend to be more harmful in applications. In addition, the mean squared prediction error of the classifier, or Brier score (Brier, 1950), can be decomposed into terms corresponding to the squared ℓ_2 calibration error and the variance of the model's correctness likelihood (Kuleshov & Liang, 2015; Kumar et al., 2019).

2.1 Estimates of Calibration Error

To estimate the TCE of a model f, assume we are given a dataset containing n samples, $\{x_i, y_i\}_{i=1}^n$. We can approximate TCE by replacing the outer expectation in Equation 1 by the sample average and replacing the inner expectation with an average over a set of instances with similar $f(x)$ values:

$$\text{ECE}_{\text{NEIGH}}(f) = \left(\frac{1}{n}\sum_{i=1}^n \left|f(x_i) - \frac{1}{|\mathcal{N}_i|}\sum_{j \in \mathcal{N}_i} y_j\right|^p\right)^{\frac{1}{p}}, \tag{2}$$

where $\mathcal{N}_i$ is instance i's set of neighbors in model confidence output space.

Label-binned calibration error (ECE_{LB}). The label-binned calibration error uses binning to define $\mathcal{N}_i$ and estimate the model's empirical accuracy $\mathbb{E}[Y|f(X)]$. Specifically, the instances are partitioned into b bins, where B_k denotes the set of all instances in bin k, allowing us to express Equation 2 in terms of the binned neighborhood:

$$\text{ECE}_{\text{LB}}(f) = \left(\frac{1}{n}\sum_{k=1}^b \sum_{i \in B_k} |f(x_i) - \bar{y}_k|^p\right)^{\frac{1}{p}}, \text{ where } \bar{y}_k = \frac{1}{|B_k|}\sum_{j \in B_k} y_j. \tag{3}$$

Binning is commonly implemented using either *equal width binning* (Guo et al., 2017; Naeini et al., 2015), which creates bins by dividing the model confidence domain $[0, 1]$ into equal sized intervals, or *equal mass binning* (Nixon et al., 2019), which creates bins by dividing the n samples into partitions with an equal number of instances.

Binned calibration error (ECE_{BIN}). In contrast to ECE_{LB}, which operates on the original instances but uses binning to estimate empirical accuracy, ECE_{BIN} collapses all instances in a bin into a single instance and compares the per-bin empirical accuracy to the per-bin confidence score, weighted by the per-bin number of instances. Given b bins, where B_k is the set of instances in bin k, and letting $\bar{f}_k$ and $\bar{y}_k$ be the per-bin average confidence score and label, ECE_{BIN} is defined under the ℓ_p norm as

$$\text{ECE}_{\text{BIN}}(f) = \left(\sum_{k=1}^{b} \frac{|B_k|}{n} \left|\bar{f}_k - \bar{y}_k\right|^p\right)^{\frac{1}{p}} \tag{4}$$

Importantly, ECE_{BIN} always underestimates ECE_{LB}, $\text{ECE}_{\text{LB}}(f) \geq \text{ECE}_{\text{BIN}}(f)$, which follows by applying Jensen's inequality on each inner term $k \in \{1, 2, \ldots, b\}$ in Eqs. 3 and 4:

$$\frac{1}{|B_k|} \sum_{i \in B_k} |f(X_i) - \bar{Y}_k|^p \geq \left|\sum_{i \in B_k} \bar{f}_k - \bar{Y}_k\right|^p. \tag{5}$$

3 Measuring bias through simulation

We focus on bias rather than variance because the variance can be estimated from a finite set of samples through resampling techniques whereas the bias is an unknown quantity that reflects systematic error. We also found empirically that the variance seems relatively insensitive to the estimation technique and number of bins (see Appendix B). The *bias* of a calibration error estimator, $\text{ECE}_{\mathcal{A}}$ for some estimation algorithm $\mathcal{A}$, is the difference between the estimator's expected value with respect to the data distribution and the TCE:

$$\text{Bias}_{\mathcal{A}} = \mathbb{E}[\text{ECE}_{\mathcal{A}}] - \text{TCE}. \tag{6}$$

If we assume a particular confidence score distribution $\mathcal{F}$ and true calibration curve $T(X) = \mathbb{E}_Y[Y \mid f(X) = c]$ (see Figure 1b for examples), we can compute the TCE by numerically evaluating the integral implicit in the outer expected value of Equation 1.

We then compute a sample estimate of the bias as follows. First, we generate n samples $\{f(x_i), y_i\}_{i=1}^n$ such that $f(x_i) \sim \mathcal{F}$ and $\mathbb{E}_Y[Y \mid f(X) = c] := T(c)$, and compute the ECE on the sample. We repeat this process for m simulated datasets and compute the sample estimate of bias as the difference between the average ECE and the TCE:[2]

$$\widehat{\text{Bias}}_{\mathcal{A}}(n) = \frac{1}{m} \sum_{i=1}^{m} \text{ECE}_{\mathcal{A}} - \text{TCE}. \tag{7}$$

Bias in ECE_{BIN} for varying hyperparameters. Using simulation, we next investigate the bias in ECE_{BIN} as a function of the number of samples n and the number of bins. We compute ECE_{BIN} with equal width binning and we assume parametric curves for $f(x)$ and $\mathbb{E}_Y[Y \mid f(X) = c]$ that are fit to the ResNet-110 CIFAR-10 model output (see Section 5.1 for details on how we compute fits). Kumar et al. (2019) Proposition 3.3 shows that any binned version of calibration error systematically underestimates TCE *in the limit of infinite data*. However, for a finite number of samples n, Figure 2 shows that ECE_{BIN} can either overestimate or underestimate TCE and that increasing the number of bins does not always lead to better estimates of TCE. Intuitively, as the number of bins explodes, each example lies in its own bin, and the prediction error is computed with respect to a target of 0 or 1. Moreover, regardless of binning scheme, there exists a bin number for each sample size that results in the lowest estimation bias and this optimal bin count grows with the sample size. In Appendix B, we show the variance associated with this experiment, and also include results for alternative calibration metrics.

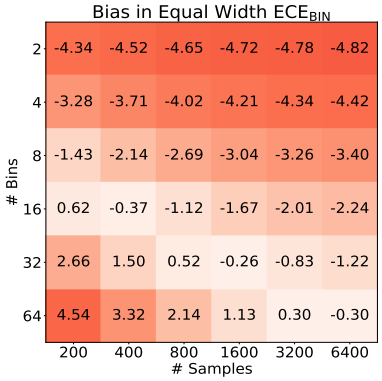

Figure 2: **ECE_{BIN} with equal width binning can overestimate TCE and the optimal number of bins depends on number of samples.**

[2]In the remainder of the text, we will use the term "bias" to refer to this sample estimate of bias.

4 MONOTONIC CALIBRATION METRICS

Though Section 3 shows that there exists an optimal number of bins for which ECE_{BIN} has the lowest bias, unfortunately, this number depends on the binning technique, the number of samples, the confidence score distribution, and the true calibration curve. This observation motivates us to seek a method for adaptively choosing the number of bins.

Monotonicity in the true calibration curve implies that a model's expected accuracy should always increase as the model's confidence increases. Although such a requirement seems reasonable for most any statistical model, it is not obvious how to prove why or when a "reasonable" model would attain such a property. We offer a rationale for why it should be expected of machine learning models trained with a maximum likelihood objective, e.g., cross-entropy or logistic loss (Murphy, 2012). Namely, from ROC (receiver operating characteristic) analysis of maximum likelihood models, an under-appreciated observation of ROC curves is that a model trained to maximize the likelihood ratio must have a convex ROC curve in the limit of infinite data (Green et al. (1966), Section 2.3). The slope of the ROC curve is related to the calibration curve, and a convex ROC curve implies a monotonically increasing calibration curve (the converse is also true) (Chen et al., 2018; Gneiting & Vogel, 2018).

In practice, several potential confounds may lead to measuring a non-monontonic calibration curve. First, finite data size effects may lead to fluctuations in the true positive or false positive rates, but do not reflect the behavior of the underlying model. Second, deviations in the domain statistics between cross-validated splits in the data may lead to unbounded behavior; however, we assume that such domain shifts are negligible as cross-validated splits are presumed to be selected *i.i.d.*.[3] Given that deviations from non-monotonic calibration curves are considered artificial, we posit that any method that is trying to assess the TCE of an underlying model may freely assume monotonicity in the true calibration curve. Note that this proposition already guides the entire field of re-calibration to require that re-calibration methods only consider monotonic functions (Platt et al., 1999; Wu et al., 2012; Zadrozny & Elkan, 2002).

Monotonic sweep calibration error ($\text{ECE}_{\text{SWEEP}}$). Accordingly, we leverage the underlying monotonicity in the true calibration and we develop the monotonic sweep calibration error to choose the largest number of bins possible such that it and all smaller bin sizes preserve monotonicity in the bin heights $\bar{y}_k$.

$$\text{ECE}_{\text{SWEEP}} = \max_b \left(\left(\sum_{k=1}^{b'} \frac{|B_k|}{n} \left| \bar{f}_k - \bar{y}_k \right|^p \right)^{\frac{1}{p}} \quad \text{s.t. } \bar{y}_1 \leq \bar{y}_2 \ldots \leq \bar{y}_{b'}, \ \forall b' \leq b \right).$$

We can compute the monotonic sweep calibration error by starting with $b = 2$ bins (since $b = 1$ is guaranteed to be a monotonic binning) and gradually increasing the number of bins until we either reach a non-monotonic binning, in which case we return the last b that corresponded to a monotonic binning, or until every sample belongs to its own bin ($b = n$).

Algorithm 1: Monotonic Sweep Calibration Error

```
for b ← 2 to n do
    Compute ECE_BIN bin heights (ȳ_k) with b bins ;
    if Binning is not monotonic then
        b = b -1 ;
        break ;
return ECE_BIN computed with b bins
```

[3]Note that a third potential reason for a non-monotonic calibration curve is that a classifier could be trained with a non–likelihood-based statistical criteria, e.g. moment matching. However, the lack of monotonic behavior in the calibration curve of such a model may actually be a sign that the model is not reasonable or admissible model for consideration on a given task (Chen et al., 2018; Pesce et al., 2010).

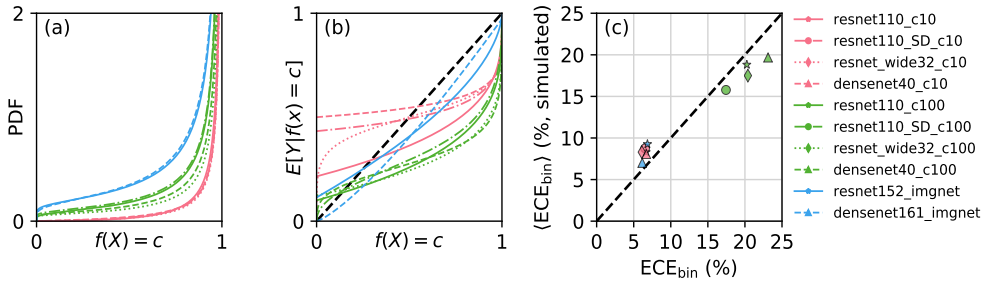

Figure 3: **Maximum likelihood fits to empirical datasets illustrate large skew in their density distribution and calibration function**. For each dataset, (a) confidence distributions were fit with a two-parameter beta distribution and (b) calibration curves were fit via generalized linear models across multiple model families, with the best model selected via the Akaike information criterion (details in Appendix A). Across models, the dataset source systematically affects both curves. (c) We plot the overall quality of the fits by computing the $\mathrm{ECE_{BIN}}$ on the original data vs. the $\mathrm{ECE_{BIN}}$ averaged over 1000 simulated trials. Curves well-fit to the data should lie close to the identity line.

5 Results

5.1 Parametric fits capture calibration curve and score distribution

TCE is analytically computable when we assume parametric forms for the confidence distribution and the true calibration curve. To what extent can parametric forms capture the diversity and complexity of real world data? In many applications, only sample-based approximations to these functions are available. In order to estimate $\mathrm{ECE_{BIN}}$ bias in real-world data, we develop parametric models of empirical logit datasets that enable direct measurement of TCE.

We consider 10 logit datasets (including those studied in Guo et al. (2017)), arising from training four different neural model families (ResNet, ResNet-SD, Wide-ResNet, and DenseNet) on three different image datasets (CIFAR-10/100 and ImageNet) (Deng et al., 2009; He et al., 2016; Huang et al., 2016; 2017; Krizhevsky, 2009; LeCun et al., 1998; Zagoruyko & Komodakis, 2016). For each dataset (Figure 3), we compute confidence scores by applying softmax and top-1 selection to logits from Kängsepp (2019).

Computing TCE directly for real-world data via Equation 1 is infeasible because of the expectation across X. Instead, we model the distribution of the scores $f(X)$ directly with a two-parameter beta distribution, which we fit using maximum likelihood estimation (note that in many cases, the confidence scores are heavily skewed). Calibration functions are computed by fitting multiple (binary) generalized linear models (GLM) to the calibration data. From these candidate models, we select the model of best fit using the Akaike Information Criteria (AIC). The models considered include logit, log, and "logflip" ($\log(1-x)$) link and transformation functions, up to first order in the transformed domain, resulting in monotonic calibration functions. See Appendix A for additional details.

We find that the parametric forms for the calibration curve and distribution of scores are well captured by these simple GLM and Beta models. Figure 3(a,b) shows the resulting fits, with parameters summarized in Tables 1 and 2. We observe significant skew in the score distribution which, as discussed in Section 5.2, poses a challenge to measuring calibration error with equal-width bins. We find that the dataset has more influence on the fits than the neural model, with ImageNet models the least skewed and CIFAR-10 the most (correlating with model accuracy). Figure 4 3(c) indicates that $\mathrm{ECE_{BIN}}$ scores computes on simulated data from the fits closely match $\mathrm{ECE_{BIN}}$ scores computed on the real data, as witnessed by the fact that the points lie near the line of equality.

5.2 Simulation results on distributions fit to CIFAR-10/100, and ImageNet

Using the resulting parametric fits from Section 5.1, we evaluate $\mathrm{ECE_{BIN}}$ and $\mathrm{ECE_{SWEEP}}$ using both equal mass binning and equal width binning and compare these values to the analytically computed TCE. We choose 15 bins for $\mathrm{ECE_{BIN}}$, following the standard set by Guo et al. (2017). In addition, we include a comparison to (Kumar et al., 2019)'s debiased estimator using equal mass binning and a

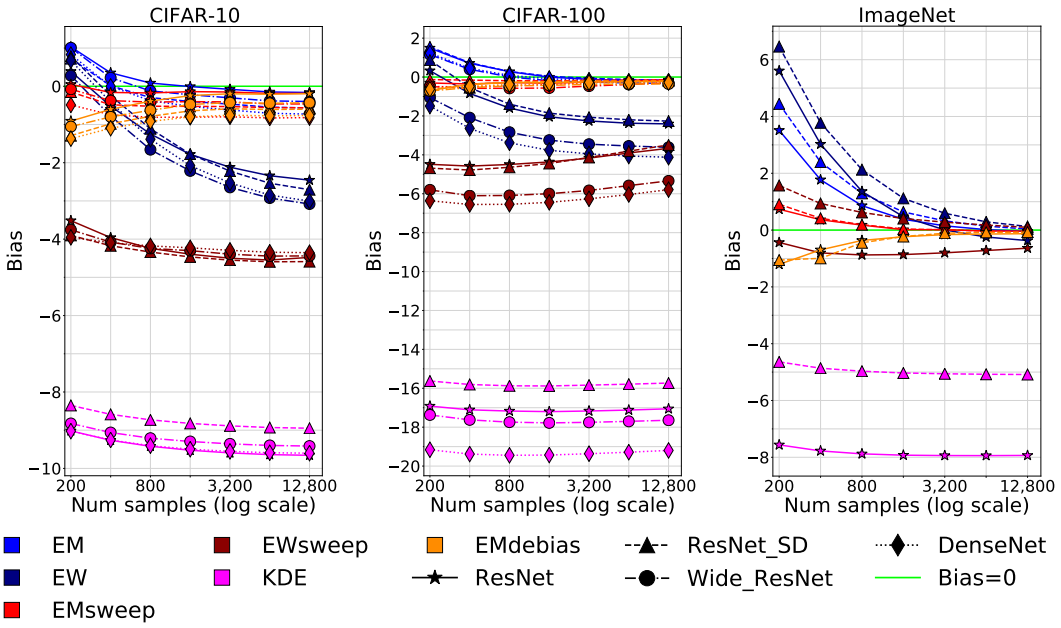

Figure 4: **`EMsweep` is less biased than alternative calibration metrics.** We plot bias versus number of samples n for calibration metrics on simulated data drawn from the CIFAR-10, CIFAR-100, and ImageNet fits (Section 5.1). The dataset the model was trained on has a greater influence on bias than the model architecture. Metrics based on equal mass binning consistently outperform equal width binning. Exploiting monotonicity in the `EMsweep` metric helps the most at small sample sizes.

smoothed Kernel Density Estimation (KDE) method for estimating calibration error (Zhang et al., 2020). We abbreviate each method as follows:

- `EW`: ECE_{BIN} using equal width binning and 15 bins (Guo et al., 2017; Naeini et al., 2015),
- `EM`: ECE_{BIN} using equal mass binning and 15 bins (Nixon et al., 2019),
- `EMdebias`: Debiased calibration metric using equal mass binning (Kumar et al., 2019)
- `KDE`: KDE calibration metric (Zhang et al., 2020)
- `EWsweep`: $\text{ECE}_{\text{SWEEP}}$ using equal width binning, and
- `EMsweep`: $\text{ECE}_{\text{SWEEP}}$ using equal mass binning.

For a given machine learning dataset and neural network model, we calculate the ECE as follows. We generate $m = 1{,}000$ simulated datasets containing n samples each drawn such that the confidence score distribution $\mathcal{F}$ matches the neural model's best fit Beta distribution and the true calibration curve $\mathbb{E}_Y[Y \mid f(X) = c]$ matches the neural model's best fit GLM. Since we know the parametric form of $\mathcal{F}$ and $\mathbb{E}_Y[Y \mid f(X) = c]$, we can also analytically compute the TCE for the neural network model. Finally, we compute the bias in the calibration error estimation given by Equation 7

Figure 4 plots the bias versus the sample size n for the best-fit curves for each neural network model trained on the CIFAR-10, CIFAR-100, and ImageNet datasets. An unbiased estimator would have Bias $= 0$, which we highlight visually in green. We find that the dataset the model was trained on has more influence on the calibration metric behavior than the model architecture. This may be unsurprising given that Section 5.1 shows that the dataset heavily influences both the distribution of confidence scores and the true calibration curve.

Equal width versus equal mass binning: Overall, metrics that employ equal mass binning show less bias than those with equal width binning. Surprisingly, for `EW` and `EWsweep` on CIFAR-10, as well as `EW` on CIFAR-100, we see increasing absolute bias as the number of samples increases across all model architectures tested. We propose a possible explanation for this phenomenon. As Figure 3 (a) shows, models trained on CIFAR-10 and CIFAR-100 have highly skewed confidence distributions and, as a result, equal width binning places the majority of the instances in the top bin. As we increase

the number of samples, we increase the likelihood that we generate a sample that populates one of the lower bins, which, due to their low sample density, may have a poorer average estimate of the TCE.

ECE_{SWEEP} versus ECE_{BIN}: Our experiments show that $\text{ECE}_{\text{SWEEP}}$ with equal mass binning is consistently less biased than ECE_{BIN}, and we see the most improvements for low sample sizes. However, the $\text{ECE}_{\text{SWEEP}}$ does not show improvements over ECE_{BIN} when combined with equal width binning, and we do not recommend using the combination in practice.

5.3 BIAS VERSUS TRUE CALIBRATION ERROR

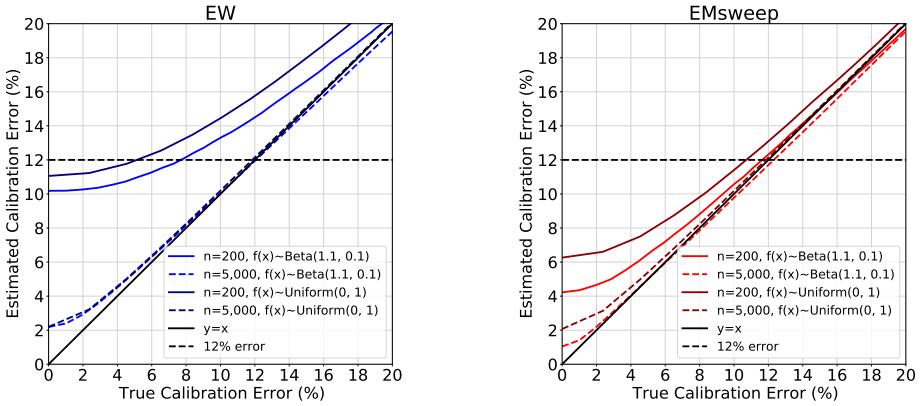

Figure 5: **Bias in calibration estimation increases as TCE decreases.** We plot the average estimated calibration error (%) for `EW` (left) and `EMsweep` (right) versus the TCE (%), with varying sample size and score distributions. The estimator bias is systematically worse for better calibrated models, and the effect is more egregious with fewer samples. At $n = 200$ samples, depending on the score distribution, an `EW` estimate of 12% could either correspond to 5% or 8% TCE. The `EMsweep` metric is able to mitigate the bias and ambiguity in calibration error estimation to a certain extent.

We next evaluate the estimation bias of the baseline `EW` and our best estimator from the previous section, `EMsweep`, as we systematically vary the TCE. We are interested in the low calibration error regime because a goal of many recalibration algorithms is to reduce the calibration error of the model to 0%. Figure 13 shows the average estimated calibration error for `EW` and `EMsweep` versus the TCE. The average calibration error is computed across $m = 1{,}000$ simulated datasets, and we include results for two sample sizes, $n = 200$ and $n = 5{,}000$, and two score distributions, $f(x) \sim \text{Uniform}(0, 1)$ and $f(x) \sim \text{Beta}(1.1, 0.1)$, the beta distribution fit to the CIFAR-100 Wide ResNet_32. To control the TCE, we assume $\mathbb{E}_Y[Y \mid f(X) = c] = c^d$ and vary $d \in [1, 10]$. When $d = 1$ the true calibration curve is $\mathbb{E}_Y[Y \mid f(X) = c] = c$, which means the model's predicted confidence score is exactly equal to its empirical accuracy and thus the TCE is 0%. As we increase d, we move the true calibration curve farther away from the perfect calibration curve, which increases the TCE of the model.

The bias in the calibration error estimation can be seen visually as the difference between the ECE and the TCE. Perfect estimation (0 bias) corresponds to the $y = x$ line. Bias is highest when the model is perfectly calibrated (TCE is 0%) and generally decreases as TCE increases. Using a larger sample size of $n = 5,000$ reduces the bias, but when the model is perfectly calibrated, the ECE_{BIN} can still be off by 2%. The `EMsweep` metric significantly reduces this bias.

In practice, we do not know the distribution of scores $\mathcal{F}$, the true calibration curve $\mathbb{E}_Y[Y \mid f(X) = c]$, or the TCE. So, given a measurement of calibration error, how much bias can we expect? If we measure an ECE_{BIN} of 20%, we expect it to be fairly close to the TCE. However, if we see an ECE_{BIN} of 2%, it is possible that the model may actually be perfectly calibrated! We further explore this dilemma in the next section.

5.4 HOW WELL CAN WE DETECT MISCALIBRATION?

Consider the situation where we have a model whose TCE is unknown and we wish to test the hypothesis that the model is miscalibrated, i.e., TCE > 0. Our ability to detect miscalibration depends on the TCE, the sample size (n), and the method for estimating calibration error. We conduct a

simulation with $f(x) \sim \text{Beta}(1, 1)$ and true calibration curve from the family $\mathbb{E}_Y[Y \mid f(X) = c] = c^d$, where d is varied to obtain a range of TCE. Allowing for a type I error rate of .05 (also known as the false-alarm rate, or the rate of mistakenly claiming miscalibration when a model is perfectly calibrated), we obtain type II error rates (also known as the miss rate, or the rate of failing to detect a miscalibration). Figure 6 shows the type II error rate as a function of TCE and n for `EMsweep` and `EW`. Our results indicate that `EMsweep` obtains a significantly lower failure rate than `EW`, particularly for under 10,000 samples. More generally, we note limitations with both methods: to detect a miscalibration of 2%, over 10,000 samples are needed; and if one has under 500 samples, the miscalibration must be greater than 10% to be detected reliably.

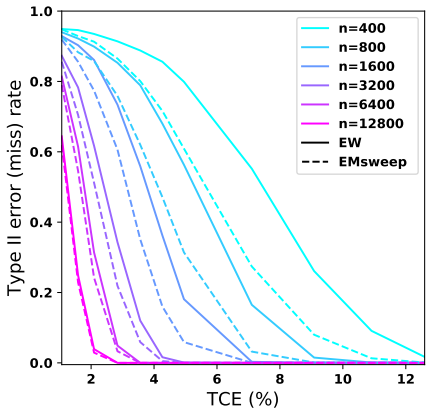

Figure 6: **Probability of failing to detect miscalibration (type II error, or miss rate),** plotted as a function of TCE for various sample sizes (n), with type I error rate fixed at 0.05. `EMsweep` (dashed lines) obtains a significantly lower failure rate than `EW` (solid lines).

6 Discussion

Much research in model calibration has focused on recalibrating models, i.e., transforming $f(x)$ to $f'(x)$ (Platt et al., 1999; Zadrozny & Elkan, 2001; 2002). We focus on estimating calibration error, because without a good estimate of TCE, there is little point in trying to recalibrate models. What implications do our results have on choosing and evaluating recalibration algorithms?

One possibility is that bias affects all recalibration methods in the same way, which would imply that we should still be able to select recalibration method A over method B with a biased estimator. However, our results show that the distribution of confidence scores significantly impacts the bias in calibration error estimation, even when the sample size is fixed. Since recalibration methods are inherently designed to modify the confidence score distribution, we cannot assume that bias will affect all methods in the same way.

Another possibility is that the bias is small compared to the calibration error differences we would measure. However, our results suggest that this is not true. Even when the number of evaluation samples is high, $n = 5,000$, Figure 13 shows that it is entirely possible that we might measure an ECE_{BIN} of 2% when the model is in fact perfectly calibrated. For comparison, in the experimental evaluations of Guo et al. (2017), the best recalibration method for a CIFAR-10 ResNet110 is only better by 0.04% ECE_{BIN}. Thus, the bias in calibration error estimation could easily overshadow differences between recalibration algorithms.

Several authors attempt a different approach to recalibration: improving model calibration during training. For instance, Mukhoti et al. (2020) trains a model with a batch size of 128 across multiple types of losses including maximum mean calibration error (Kumar et al., 2018) and Brier loss (Brier, 1950) which explicitly tries to minimize a calibration loss using 128 examples at a time. However, our results suggest that training a model with naive estimates of calibration error as an objective using a batch size $< O(1000)$ is a potentially flawed endeavor, particularly because the distribution of scores from the model is changing throughout training, and any potential measure of calibration may be more affected by the distribution of scores (as opposed to the calibration curve).

7 Related Work

Sensitivity of ECE_{BIN} to hyperparameters. Several works have pointed out that ECE_{BIN} is sensitive to implementation details. Kumar et al. (2019) show that ECE_{BIN} increases with number of bins while Nixon et al. (2019) find that ECE_{BIN} scores are sensitive to several hyperparameters, including ℓ_p norm, number of bins, and binning technique. In addition, Nixon et al. (2019) find that ECE_{BIN} with equal mass binning produces more stable rankings of recalibration algorithms, which is consistent with our conclusion that equal mass ECE_{BIN} is a less biased estimator of TCE. However, in contrast to prior work, we study the sensitivity of the *bias* in ECE_{BIN} to implementation hyperparameters.

Metrics for calibration error estimation. Gupta et al. (2020) propose a calibration error metric inspired by the Kolmogorov-Smirnov (KS) statistical test that estimates the maximum difference between the cumulative probability distributions $P(f(X))$ and $P(Y \mid f(X))$. The KS is similar to the maximum calibration error (MCE) (Naeini et al., 2015) in that it computes a worst-case deviation between confidence and accuracy, but the KS is computed on the CDF, while the MCE uses binning and is computed on the PDF. In contrast, our work focuses on measuring the *average* difference between confidence and accuracy. As mentioned in Guo et al. (2017), both the worst case and average difference are useful measures but may be applicable under different circumstances.

8 Conclusions and Future Work

If we are to rely on the predictions from machine learning models in high stakes situations like autonomous vehicles, content moderation, and medicine, we must be able to detect when these predictions are likely to be incorrect. Given that the default confidence scores produced by machine learning models do not necessarily correspond to the model's empirical accuracy, recalibration is necessary in order to produce reliable and consistent output. However, it is impossible for a recalibration algorithm to achieve perfect calibration if we cannot measure calibration accurately. Our results show that the statistical bias in current calibration error estimators grows as we approach perfect calibration, but this bias can be mitigated by using monotonic estimation techniques. We conclude with some directions for future work:

Simulation as an evaluation tool. We have shown that simulation is a powerful technique for evaluating calibration error estimators. However, especially for small sample sizes, the $\text{ECE}_{\text{SWEEP}}$ method does not completely eliminate estimation bias, and we only evaluated a finite set of distributions arising from image classification datasets and models. We hope future work can use simulation as an effective tool for developing both new calibration metrics and new recalibration techniques, and that evaluations can be extended to a more diverse set of datasets and models.

Distribution shifts. Since models deployed in real world application will necessarily make predictions on out-of distribution examples and since we would like these predictions to be calibrated (Ovadia et al., 2019), it is important that we are able to accurately measure and improve calibration error on non-iid data. However, in such situations, we do not necessarily expect the calibration curve to be monotonic. Thus, exploring how distribution shifts can modify the shape of the true calibration curve is an important future direction.

References

Aharon Azulay and Yair Weiss. Why do deep convolutional networks generalize so poorly to small image transformations? *arXiv preprint arXiv:1805.12177*, 2018.

Battista Biggio and Fabio Roli. Wild patterns: Ten years after the rise of adversarial machine learning. *Pattern Recognition*, 2018. `https://arxiv.org/abs/1712.03141`.

Glenn W Brier. Verification of forecasts expressed in terms of probability. *Monthly weather review*, 78(1):1–3, 1950.

Holger Caesar, Varun Bankiti, Alex H Lang, Sourabh Vora, Venice Erin Liong, Qiang Xu, Anush Krishnan, Yu Pan, Giancarlo Baldan, and Oscar Beijbom. nuscenes: A multimodal dataset for autonomous driving. In *Proceedings of the IEEE/CVF Conference on Computer Vision and Pattern Recognition*, pp. 11621–11631, 2020.

Weijie Chen, Berkman Sahiner, Frank Samuelson, Aria Pezeshk, and Nicholas Petrick. Calibration of medical diagnostic classifier scores to the probability of disease. *Statistical methods in medical research*, 27(5):1394–1409, 2018.

J. Deng, W. Dong, R. Socher, L.-J. Li, K. Li, and L. Fei-Fei. ImageNet: A Large-Scale Hierarchical Image Database. In *CVPR09*, 2009.

Andre Esteva, Brett Kuprel, Roberto A Novoa, Justin Ko, Susan M Swetter, Helen M Blau, and Sebastian Thrun. Dermatologist-level classification of skin cancer with deep neural networks. *nature*, 542(7639):115–118, 2017.

Andre Esteva, Alexandre Robicquet, Bharath Ramsundar, Volodymyr Kuleshov, Mark DePristo, Katherine Chou, Claire Cui, Greg Corrado, Sebastian Thrun, and Jeff Dean. A guide to deep learning in healthcare. *Nature medicine*, 25(1):24–29, 2019.

Andreas Geiger, Philip Lenz, Christoph Stiller, and Raquel Urtasun. Vision meets robotics: The kitti dataset. *The International Journal of Robotics Research*, 32(11):1231–1237, 2013.

Andrew Gelman, John B. Carlin, Hal S. Stern, and Donald B. Rubin. *Bayesian Data Analysis*. Chapman and Hall/CRC, 2nd ed. edition, 2004.

Tilmann Gneiting and Peter Vogel. Receiver operating characteristic (roc) curves. *arXiv preprint arXiv:1809.04808*, 2018.

David Marvin Green, John A Swets, et al. *Signal detection theory and psychophysics*, volume 1. Wiley New York, 1966.

Varun Gulshan, Lily Peng, Marc Coram, Martin C Stumpe, Derek Wu, Arunachalam Narayanaswamy, Subhashini Venugopalan, Kasumi Widner, Tom Madams, Jorge Cuadros, et al. Development and validation of a deep learning algorithm for detection of diabetic retinopathy in retinal fundus photographs. *Jama*, 316(22):2402–2410, 2016.

Chuan Guo, Geoff Pleiss, Yu Sun, and Kilian Q Weinberger. On calibration of modern neural networks. *International Conference on Machine Learning (ICML)*, 2017. URL https://arxiv.org/abs/1706.04599.

Kartik Gupta, Amir Rahimi, Thalaiyasingam Ajanthan, Thomas Mensink, Cristian Sminchisescu, and Richard Hartley. Calibration of neural networks using splines. *arXiv preprint arXiv:2006.12800*, 2020.

Kaiming He, Xiangyu Zhang, Shaoqing Ren, and Jian Sun. Deep residual learning for image recognition. In *Computer Vision and Pattern Recognition (CVPR)*, 2016. URL https://arxiv.org/abs/1512.03385.

Dan Hendrycks and Thomas Dietterich. Benchmarking neural network robustness to common corruptions and perturbations. In *International Conference on Learning Representations (ICLR)*, 2019. https://arxiv.org/abs/1807.01697.

Gao Huang, Yu Sun, Zhuang Liu, Daniel Sedra, and Kilian Q Weinberger. Deep networks with stochastic depth. In *European conference on computer vision*, pp. 646–661. Springer, 2016.

Gao Huang, Zhuang Liu, Laurens Van Der Maaten, and Kilian Q Weinberger. Densely connected convolutional networks. In *Proceedings of the IEEE conference on computer vision and pattern recognition*, pp. 4700–4708, 2017.

A. Krizhevsky. Learning multiple layers of features from tiny images. 2009.

Volodymyr Kuleshov and Percy S Liang. Calibrated structured prediction. In *Neural Information Processing Systems (NeurIPS)*, 2015. URL http://papers.nips.cc/paper/5658-calibrated-structured-prediction.pdf.

Ananya Kumar, Percy S Liang, and Tengyu Ma. Verified uncertainty calibration. In *Neural Information Processing Systems (NeurIPS)*, 2019. URL https://arxiv.org/abs/1909.10155.

Aviral Kumar, Sunita Sarawagi, and Ujjwal Jain. Trainable calibration measures for neural networks from kernel mean embeddings. In *International Conference on Machine Learning (ICML)*, pp. 2805–2814, 2018.

Markus Kängsepp. Nn_calibration. https://github.com/markus93/NN_calibration, 2019.

Yann LeCun, Léon Bottou, Yoshua Bengio, and Patrick Haffner. Gradient-based learning applied to document recognition. *Proceedings of the IEEE*, 86(11):2278–2324, 1998.

Jishnu Mukhoti, Viveka Kulharia, Amartya Sanyal, Stuart Golodetz, Philip HS Torr, and Puneet K Dokania. Calibrating deep neural networks using focal loss. *arXiv preprint arXiv:2002.09437*, 2020.

Kevin P Murphy. *Machine learning: a probabilistic perspective*. MIT press, 2012.

Mahdi Pakdaman Naeini, Gregory F Cooper, and Milos Hauskrecht. Obtaining well calibrated probabilities using bayesian binning. In *AAAI Conference on Artificial Intelligence*. NIH Public Access, 2015. URL https://www.ncbi.nlm.nih.gov/pmc/articles/PMC4410090/.

Jeremy Nixon, Michael W Dusenberry, Linchuan Zhang, Ghassen Jerfel, and Dustin Tran. Measuring calibration in deep learning. In *CVPR Workshops*, pp. 38–41, 2019.

Yaniv Ovadia, Emily Fertig, Jie Ren, Zachary Nado, David Sculley, Sebastian Nowozin, Joshua Dillon, Balaji Lakshminarayanan, and Jasper Snoek. Can you trust your model's uncertainty? evaluating predictive uncertainty under dataset shift. In *Advances in Neural Information Processing Systems*, pp. 13991–14002, 2019.

Lorenzo L Pesce, Charles E Metz, and Kevin S Berbaum. On the convexity of roc curves estimated from radiological test results. *Academic radiology*, 17(8):960–968, 2010.

John Platt et al. Probabilistic outputs for support vector machines and comparisons to regularized likelihood methods. *Advances in large margin classifiers*, 10(3):61–74, 1999.

Benjamin Recht, Rebecca Roelofs, Ludwig Schmidt, and Vaishaal Shankar. Do imagenet classifiers generalize to imagenet? In *International Conference on Machine Learning*, pp. 5389–5400, 2019.

Pei Sun, Henrik Kretzschmar, Xerxes Dotiwalla, Aurelien Chouard, Vijaysai Patnaik, Paul Tsui, James Guo, Yin Zhou, Yuning Chai, Benjamin Caine, et al. Scalability in perception for autonomous driving: Waymo open dataset. In *Proceedings of the IEEE/CVF Conference on Computer Vision and Pattern Recognition*, pp. 2446–2454, 2020.

Christian Szegedy, Wojciech Zaremba, Ilya Sutskever, Joan Bruna, Dumitru Erhan, Ian J. Goodfellow, and Rob Fergus. Intriguing properties of neural networks. In *International Conference on Learning Representations (ICLR)*, 2013. http://arxiv.org/abs/1312.6199.

Yuan Wu, Xiaoqian Jiang, Jihoon Kim, and Lucila Ohno-Machado. I-spline smoothing for calibrating predictive models. *AMIA Summits on Translational Science Proceedings*, 2012:39, 2012.

Bianca Zadrozny and Charles Elkan. Obtaining calibrated probability estimates from decision trees and naive bayesian classifiers. In *Icml*, volume 1, pp. 609–616. Citeseer, 2001.

Bianca Zadrozny and Charles Elkan. Transforming classifier scores into accurate multiclass probability estimates. In *ACM SIGKDD International Conference on Knowledge Discovery and Data Mining*, 2002.

Sergey Zagoruyko and Nikos Komodakis. Wide residual networks. *arXiv preprint arXiv:1605.07146*, 2016.

Jize Zhang, Bhavya Kailkhura, and T Han. Mix-n-match: Ensemble and compositional methods for uncertainty calibration in deep learning. *arXiv preprint arXiv:2003.07329*, 2020.

Table 1: Parameters of best fit for distribution functions investigated in Section 5.1.

	$\hat{\alpha}$	$\hat{\beta}$
resnet110_c10	2.7752	0.0478
resnet110_SD_c10	2.1714	0.0394
resnet_wide32_c10	2.3806	0.0379
densenet40_c10	1.9824	0.0397
resnet110_c100	1.1823	0.1081
resnet110_SD_c100	1.1233	0.1147
resnet_wide32_c100	1.0611	0.0650
densenet40_c100	1.0805	0.0808
resnet152_imgnet	1.1359	0.2069
densenet161_imgnet	1.1928	0.2206

A MAXIMUM-LIKELIHOOD FITS

$$\arg\min_{\alpha,\beta} \sum_i -\ln \frac{x_i^{\alpha-1}(1-x_i)^{\beta-1}}{\frac{\Gamma(\alpha)\Gamma(\beta)}{\Gamma(\alpha+\beta)}} \tag{8}$$

Table 1 provides parameters fit to the top-scores obtained for each of 10 empirical datasets by maximum likelihood estimation. Global optimia $\hat{\alpha} \in [0, 200]$, $\hat{\beta} \in [0, 50]$ are approximately computed using a recursively-refining brute-force search until both parameters are established to within an absolute tolerance of $1\mathrm{e}{-5}$. Each step in the recursion contracts a linear sampling grid ($N = 11$) by a factor of $\gamma = .5$ centered on the previously established optimal parameter, subject to the constraints $\alpha, \beta > 0$. Experiments confirmed that the computed optima were robust to the hyperparameters N, γ.

Table 2 provides parameters fit to calibration functions. For each sample image x_i in the image dataset, define $s_i = f(x_i)$ to be the score (the output of the top-scoring logit after softmax) and $y_i \in \{0, 1\}$ to be the classification ($y_i = 1$ when the top-scoring logit correctly classified image x_i) for the sample image. The loss for the binary generalized linear model (GLM) across different combinations of link functions $g(y)$ and transform functions $t(s)$ was optimized via the standard loss (Gelman et al. (2004)):

$$\arg\min_{b_0,b_1} \sum_i -\ln p_i^{y_i}(1-p_i)^{1-y_i}, \quad p_i = g^{-1}(b_0 + b_1 t(s_i)) \tag{9}$$

For each dataset, the GLM of best fit was selected via the Akaike Information Criteria using the likelihood at the optimized parameter values.

Table 2: Parameters of best fit for calibrations functions investigated in Section 5.1.

dataset_name	glm_name	AIC	b_0	b_1
resnet110_c10	logflip_logflip_b0_b1	**2779.22**	-0.24	0.30
	logit_logflip_b0_b1	2790.40	-0.55	-0.38
	logit_logflip_b1	2827.51		-0.31
	logit_logit_b0_b1	2840.70	-0.38	0.36
	logit_logit_b1	2900.02		0.30
	logflip_logflip_b1	2932.09		0.34
	log_log_b0_b1	3221.72	-0.06	2.53
	logit_logit_b0	3799.63	1.99	
	logflip_logflip_b0	3811.98	-2.13	
	log_log_b0	3829.05	-0.13	
	logit_logflip_b0	3868.40	1.95	
	log_log_b1	4281.78		4.75
resnet110_SD_c10	logit_logflip_b0_b1	**2498.98**	-0.27	-0.35
	logit_logit_b1	2502.52		0.30
	logit_logflip_b1	2508.70		-0.30
	logit_logit_b0_b1	2538.41	-0.26	0.33
	logflip_logflip_b0_b1	2550.29	-0.36	0.27
	logflip_logflip_b1	2572.85		0.35
	log_log_b0_b1	2594.91	-0.08	1.98
	log_log_b0	3137.19	-0.19	
	logflip_logflip_b0	3150.42	-1.80	
	logit_logit_b0	3175.58	1.58	
	logit_logflip_b0	3179.67	1.56	
	log_log_b1	3697.37		3.77
resnet_wide32_c10	logit_logit_b1	**2483.34**		0.26
	logflip_logflip_b0_b1	2487.69	-0.47	0.22
	logit_logit_b0_b1	2511.39	-0.13	0.28
	logit_logflip_b0_b1	2558.45	-0.26	-0.28
	logit_logflip_b1	2586.47		-0.25
	log_log_b0_b1	2647.03	-0.12	1.87
	logflip_logflip_b1	2713.17		0.30
	log_log_b0	2981.24	-0.21	
	logflip_logflip_b0	2983.05	-1.70	
	logit_logit_b0	2989.90	1.49	
	logit_logflip_b0	3055.55	1.45	
	log_log_b1	4582.09		4.61
densenet40_c10	logit_logflip_b1	**2910.62**		-0.26
	logit_logit_b0_b1	2961.31	-0.40	0.31
	logit_logflip_b0_b1	3000.23	-0.38	-0.31
	logflip_logflip_b0_b1	3001.78	-0.31	0.24
	logit_logit_b1	3021.54		0.25
	logflip_logflip_b1	3027.78		0.31
	log_log_b0_b1	3153.38	-0.12	2.04
	log_log_b0	3531.22	-0.22	
	logflip_logflip_b0	3589.11	-1.60	
	logit_logit_b0	3601.85	1.37	
	logit_logflip_b0	3679.95	1.30	
	log_log_b1	4735.18		4.27
resnet110_c100	logflip_logflip_b0_b1	**8181.97**	-0.11	0.28
	logit_logit_b0_b1	8206.19	-0.88	0.39
	logflip_logflip_b1	8301.28		0.31
	logit_logflip_b0_b1	8371.53	-1.01	-0.40
	logit_logit_b1	8732.11		0.25
	log_log_b0_b1	8918.21	-0.16	2.35
	logit_logflip_b1	8926.99		-0.23
	logit_logflip_b0	10903.83	0.74	
	logit_logit_b0	10943.95	0.72	
	logflip_logflip_b0	10964.91	-1.12	
	log_log_b0	11002.20	-0.40	
	log_log_b1	11850.89		4.26

dataset_name	glm_name	AIC	b_0	b_1
resnet110_SD_c100	logit_logit_b0_b1	**7873.61**	-0.88	0.49
	logflip_logflip_b0_b1	7878.19	-0.09	0.35
	logflip_logflip_b1	7932.28		0.38
	logit_logflip_b0_b1	7944.61	-1.04	-0.52
	logit_logit_b1	8315.51		0.32
	log_log_b0_b1	8437.82	-0.11	2.18
	logit_logflip_b1	8510.36		-0.30
	log_log_b1	9988.07		3.30
	logit_logit_b0	10803.27	0.80	
	log_log_b0	10810.90	-0.37	
	logflip_logflip_b0	10823.15	-1.16	
	logit_logflip_b0	10834.48	0.78	
resnet_wide32_c100	logflip_logflip_b0_b1	**7183.93**	-0.13	0.21
	logit_logit_b0_b1	7219.14	-0.98	0.33
	logflip_logflip_b1	7233.51		0.25
	logit_logflip_b0_b1	7297.00	-1.06	-0.34
	logit_logit_b1	7626.21		0.19
	log_log_b0_b1	7650.97	-0.24	2.51
	logit_logflip_b1	7795.28		-0.17
	logflip_logflip_b0	8977.39	-0.98	
	logit_logflip_b0	8987.38	0.49	
	log_log_b0	9000.24	-0.49	
	logit_logit_b0	9009.51	0.49	
	log_log_b1	11911.51		5.48
densenet40_c100	logit_logit_b0_b1	**8158.28**	-0.97	0.34
	logflip_logflip_b0_b1	8229.43	-0.12	0.22
	logit_logflip_b0_b1	8267.77	-1.08	-0.35
	logflip_logflip_b1	8368.86		0.25
	logit_logit_b1	8783.50		0.19
	log_log_b0_b1	8832.20	-0.25	2.26
	logit_logflip_b1	8918.57		-0.18
	logit_logit_b0	10138.24	0.47	
	logit_logflip_b0	10182.61	0.45	
	logflip_logflip_b0	10242.15	-0.94	
	log_log_b0	10261.01	-0.50	
	log_log_b1	13322.10		5.25
resnet152_imgnet	logflip_logflip_b0_b1	**18729.85**	-0.12	0.58
	logit_logit_b0_b1	18783.22	-0.29	0.65
	log_log_b0_b1	18785.44	-0.03	1.32
	logflip_logflip_b1	18872.14		0.65
	logit_logit_b1	19074.37		0.57
	logit_logflip_b0_b1	19095.40	-0.82	-0.79
	log_log_b1	19840.25		1.53
	logit_logflip_b1	20062.10		-0.50
	logflip_logflip_b0	26935.09	-1.41	
	log_log_b0	26968.50	-0.28	
	logit_logflip_b0	27012.77	1.12	
	logit_logit_b0	27084.11	1.11	
densenet161_imgnet	log_log_b0_b1	**18202.41**	-0.03	1.27
	logit_logit_b0_b1	18460.70	-0.25	0.68
	logflip_logflip_b1	18521.48		0.67
	logflip_logflip_b0_b1	18534.07	-0.10	0.61
	logit_logit_b1	18822.25		0.60
	logit_logflip_b0_b1	18913.25	-0.77	-0.80
	log_log_b1	19493.85		1.44
	logit_logflip_b1	19562.58		-0.54
	logit_logflip_b0	26426.38	1.19	
	logflip_logflip_b0	26445.91	-1.46	
	logit_logit_b0	26519.76	1.18	
	log_log_b0	26662.65	-0.27	

Table 3: ECE reported in Figure 3(c).

	ECE_2 (%)	<ECE_2> (%, simulated)
resnet110_c10	6.67	8.42
resnet110_SD_c10	6.54	8.79
resnet_wide32_c10	6.09	8.44
densenet40_c10	6.70	8.09
resnet110_c100	20.26	18.87
resnet110_SD_c100	17.44	15.78
resnet_wide32_c100	20.40	17.53
densenet40_c100	23.12	19.69
resnet152_imgnet	6.85	9.26
densenet161_imgnet	6.15	6.87

B BIAS AND VARIANCE IN CALIBRATION METRICS

B.1 BIAS

We evaluate bias for various calibration metrics using both equal-width and equal-mass binning as we vary both the sample size n and the number of bins b. These plots should be seen as an alternative visualization to 4 where we additionally compare to different choices for the fixed number of bins b. Since the $\text{ECE}_{\text{SWEEP}}$ metrics adaptively choose a different number of bins for each sample size, we display the bin number for this metric as -1.

We find that ECE_{BIN} can overestimate the true calibration error and there exists an optimal number of bins that produces the least biased estimator that changes with the number of samples n. Additionally, equal mass binning generally results in a less biased metric than equal width binning.

CIFAR-10 ResNet-110. Figure 7 assume parametric curves for $p(f(x))$ and $\mathbb{E}_Y[Y \mid f(X) = c]$ that we obtain from maximum-likelihood fits to CIFAR-10 ResNet-110 model output.

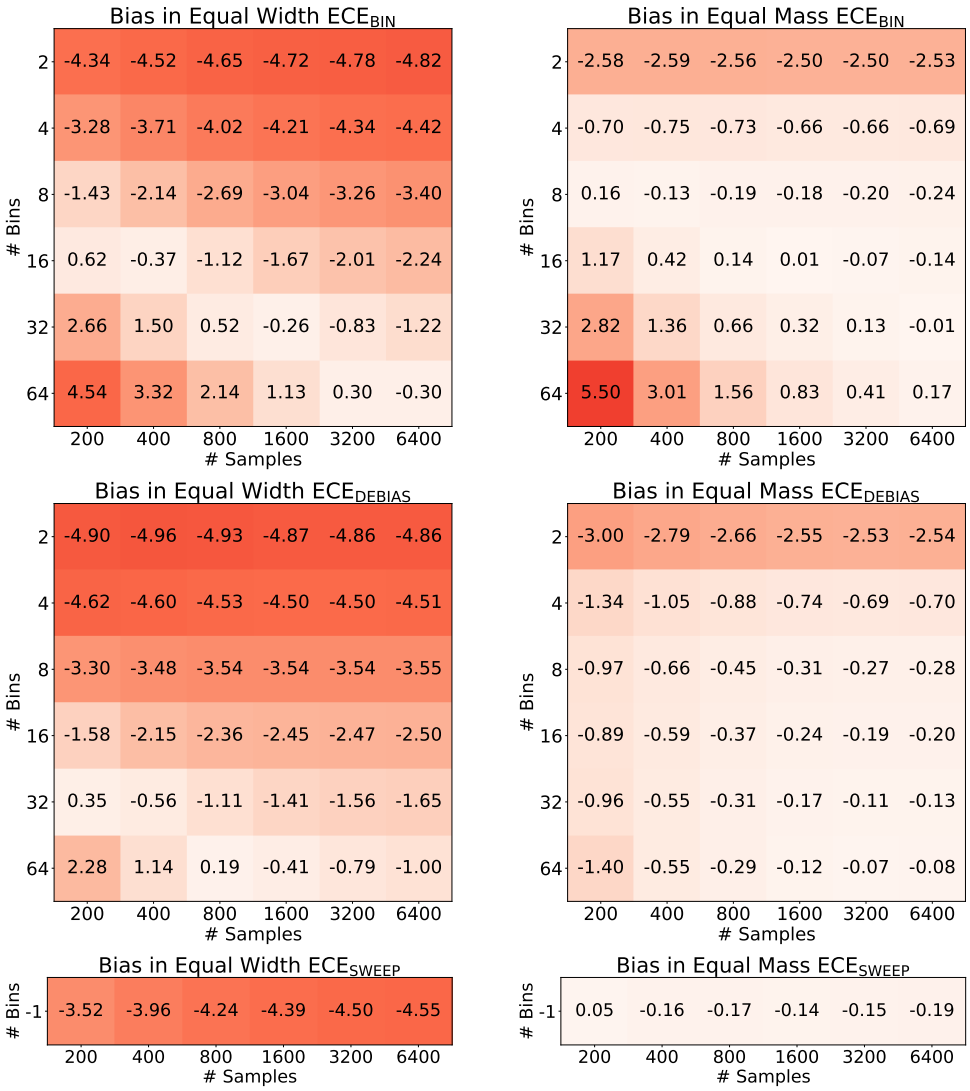

Figure 7: **Bias for various calibration metrics assuming curves fit to CIFAR-10 ResNet-110 output.** We plot bias for various calibration metrics using both equal-width binning (left column) and equal-mass binning (right column) as we vary both the sample size n and the number of bins b.

CIFAR-100 Wide ResNet-32. Figure 8 assume parametric curves for $p(f(x))$ and $\mathbb{E}_Y[Y \mid f(X) = c]$ that we obtain from maximum-likelihood fits to CIFAR-100 Wide ResNet-32 model output.

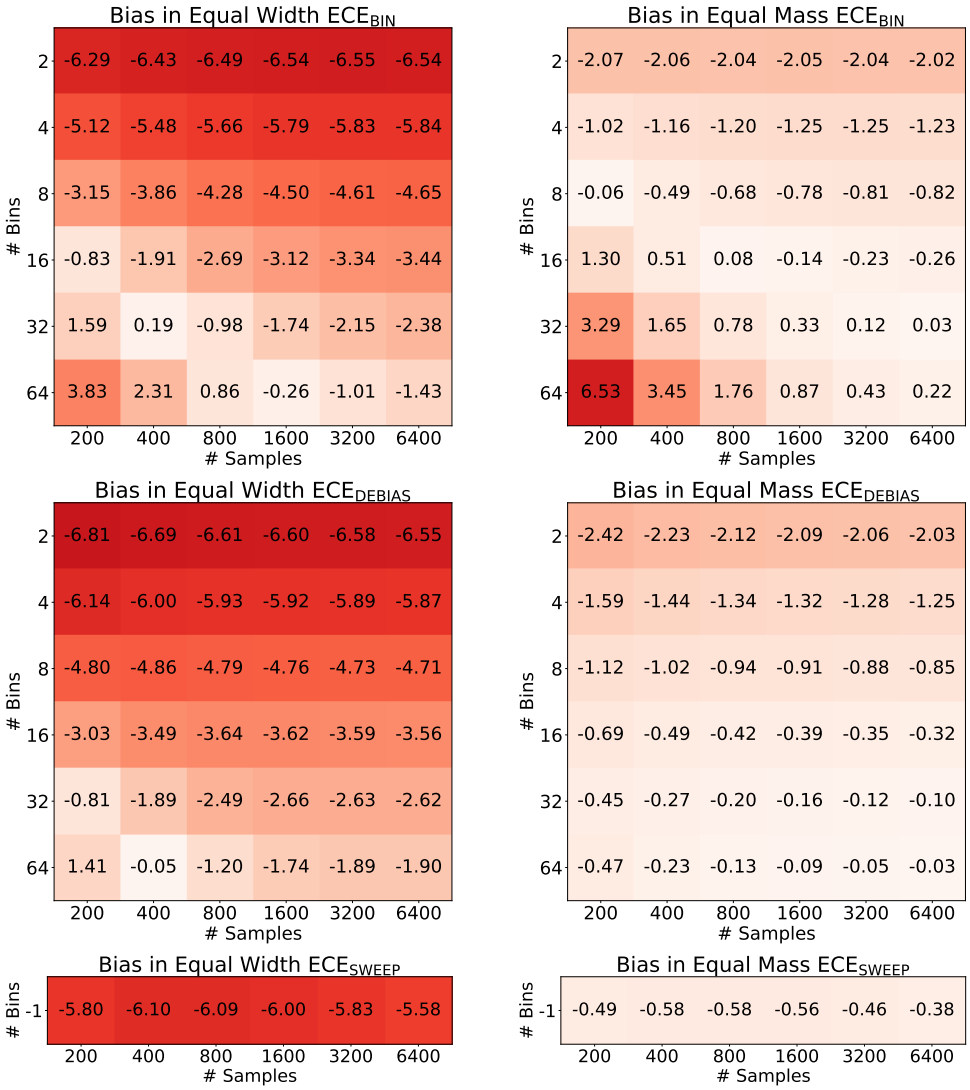

Figure 8: **Bias for various calibration metrics assuming curves fit to CIFAR-100 Wide ResNet-32 output.** We plot bias for various calibration metrics using both equal-width binning (left column) and equal-mass binning (right column) as we vary both the sample size n and the number of bins b.

ImageNet ResNet-152. Figure 9 assume parametric curves for $p(f(x))$ and $\mathbb{E}_Y[Y \mid f(X) = c]$ that we obtain from maximum-likelihood fits to ImageNet ResNet-152 model output.

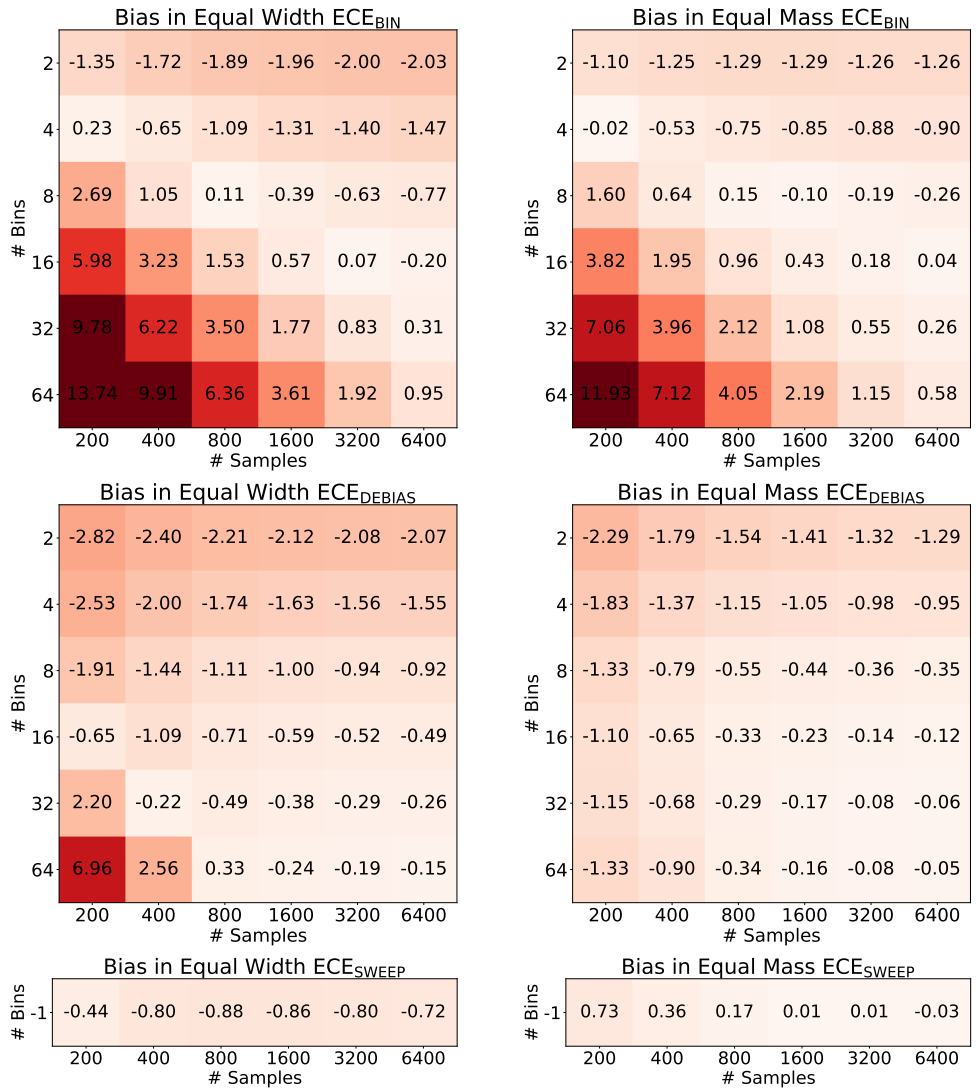

Figure 9: **Bias for various calibration metrics assuming curves fit to ImageNet ResNet-152 output.** We plot bias for various calibration metrics using both equal-width binning (left column) and equal-mass binning (right column) as we vary both the sample size n and the number of bins b.

B.2 Variance

We also compute the *variance* for various calibration metrics using both equal-width and equal-mass binning as we vary both the sample size n and the number of bins b. As expected, Figure **??** shows that variance decreases with number of samples, but, unlike the bias, there is no clear dependence on the number of bins.

CIFAR-10 ResNet-110. Figure 10 assume parametric curves for $p(f(x))$ and $\mathbb{E}_Y[Y \mid f(X) = c]$ that we obtain from maximum-likelihood fits to CIFAR-10 ResNet-110 model output.

CIFAR-100 Wide ResNet-32. Figure 11 assume parametric curves for $p(f(x))$ and $\mathbb{E}_Y[Y \mid f(X) = c]$ that we obtain from maximum-likelihood fits to CIFAR-100 Wide ResNet-32 model output.

ImageNet ResNet-152. Figure 12 assume parametric curves for $p(f(x))$ and $\mathbb{E}_Y[Y \mid f(X) = c]$ that we obtain from maximum-likelihood fits to ImageNet ResNet-152 model output.

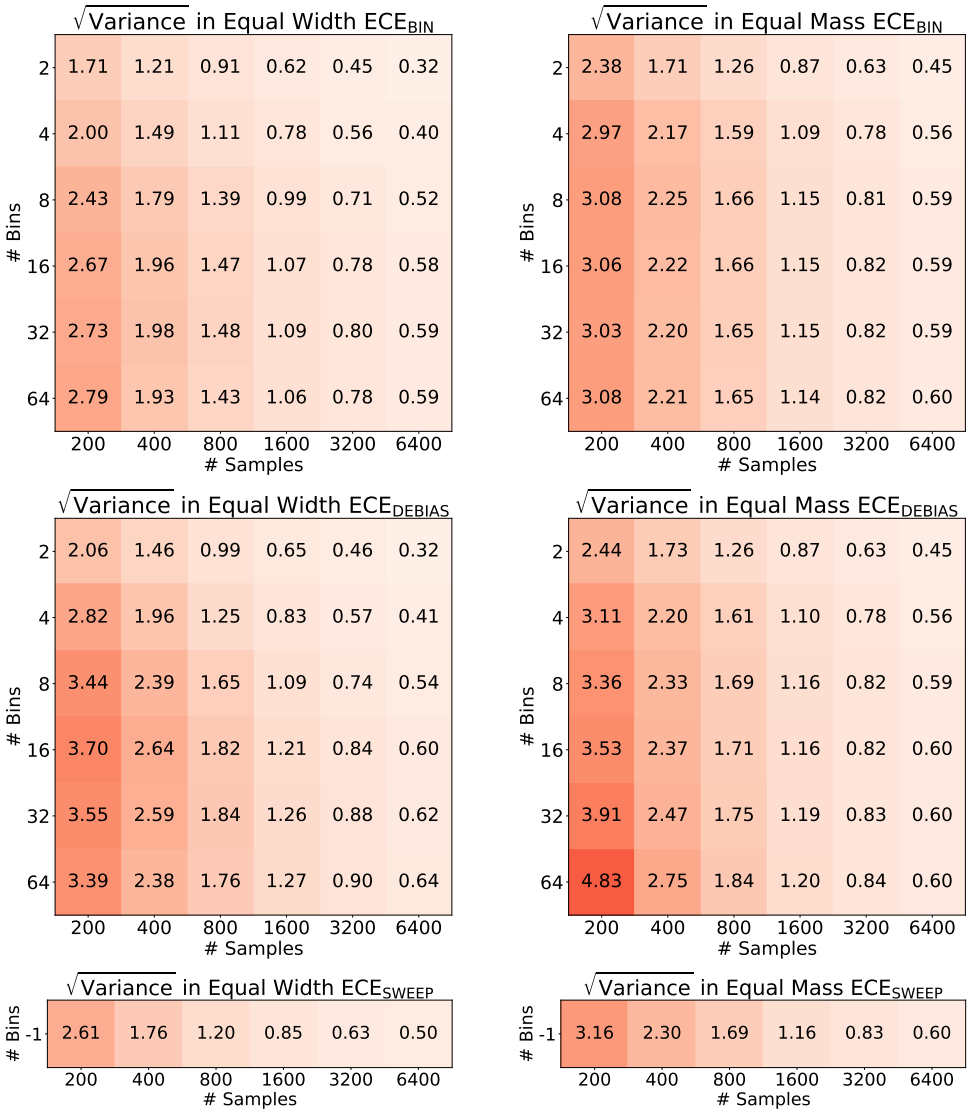

Figure 10: **$\sqrt{\text{Variance}}$ for various calibration metrics assuming curves fit to CIFAR-10 ResNet-110 output.** We plot $\sqrt{\text{Variance}}$ for various calibration metrics using both equal-width binning (left column) and equal-mass binning (right column) as we vary both the sample size n and the number of bins b.

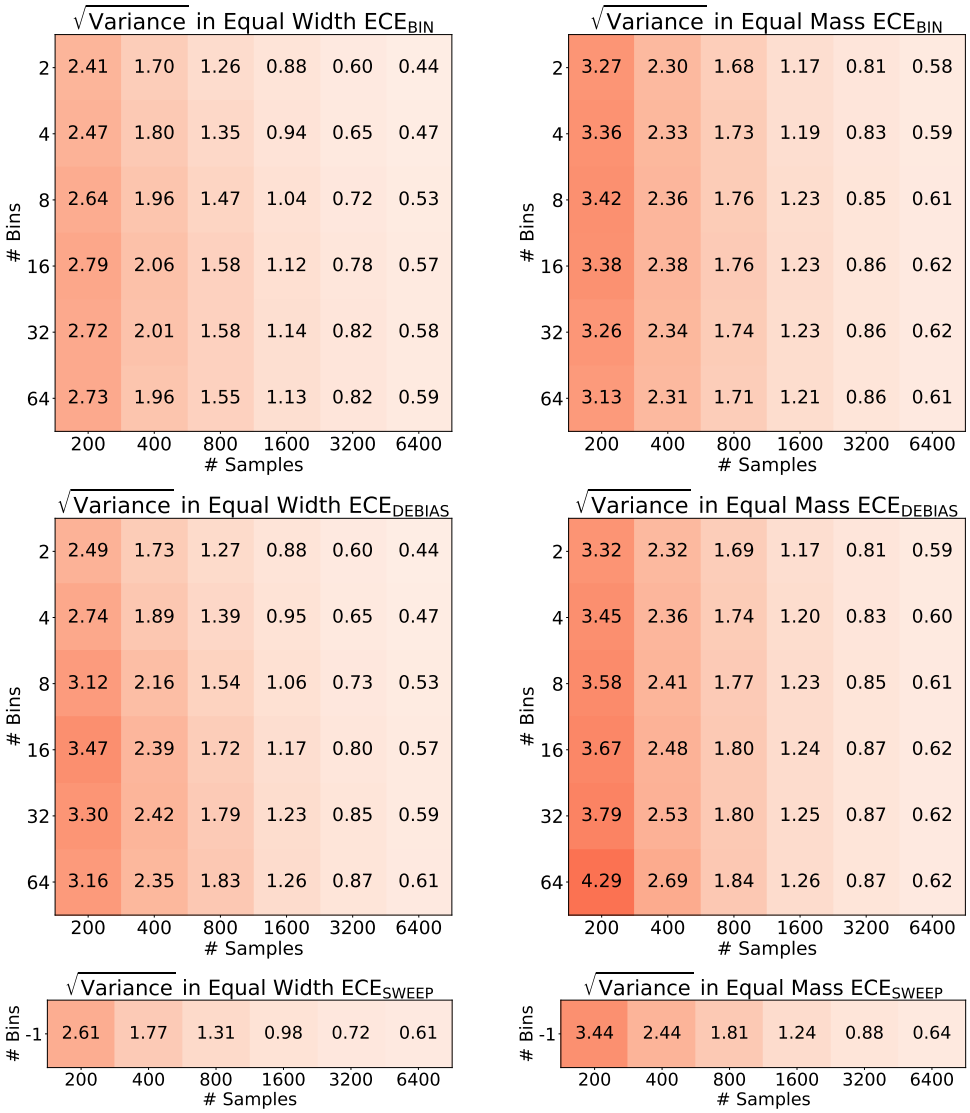

Figure 11: **$\sqrt{\text{Variance}}$ for various calibration metrics assuming curves fit to CIFAR-100 Wide ResNet-32 output.** We plot $\sqrt{\text{Variance}}$ for various calibration metrics using both equal-width binning (left column) and equal-mass binning (right column) as we vary both the sample size n and the number of bins b.

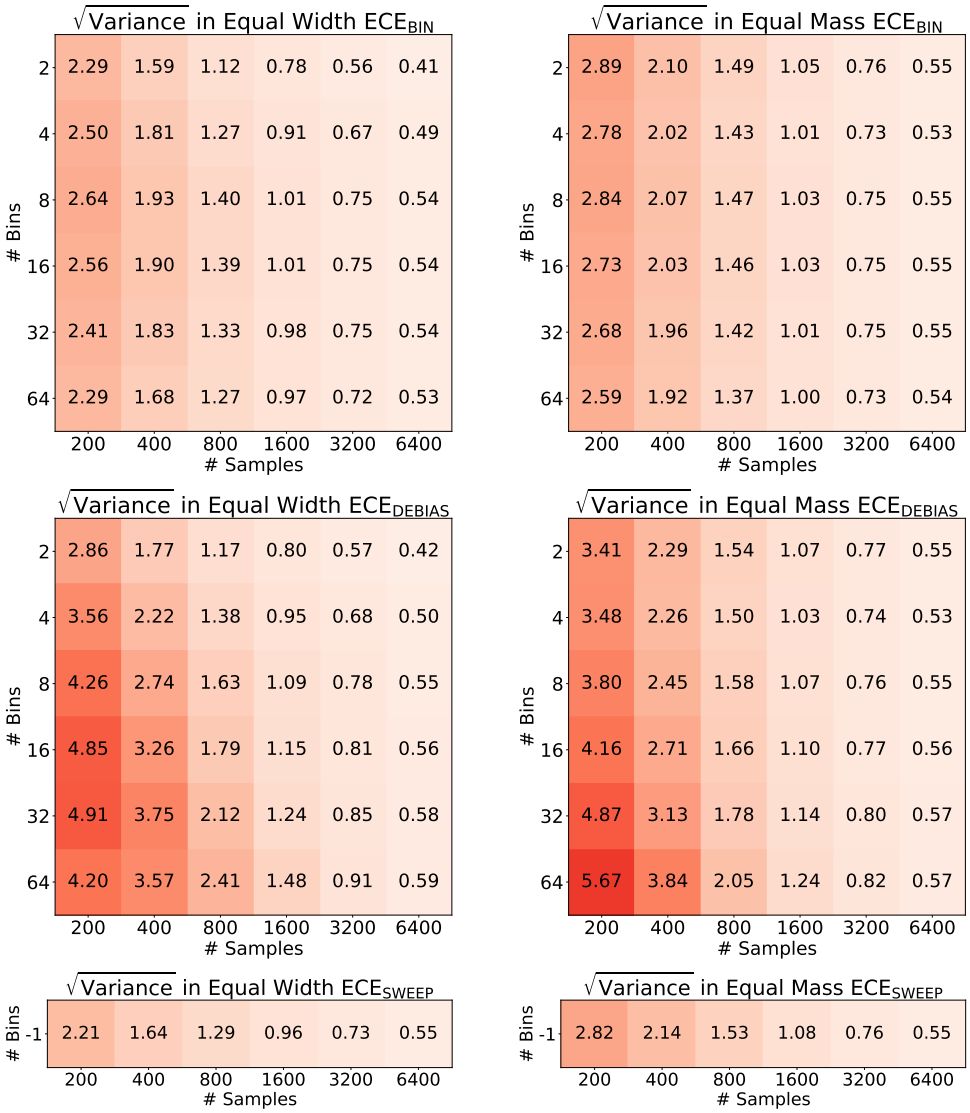

Figure 12: **$\sqrt{\text{Variance}}$ for various calibration metrics assuming curves fit to ImageNet ResNet-152 output.** We plot $\sqrt{\text{Variance}}$ for various calibration metrics using both equal-width binning (left column) and equal-mass binning (right column) as we vary both the sample size n and the number of bins b.

C WHAT NUMBER OF BINS DOES EQUAL MASS $\text{ECE}_{\text{SWEEP}}$ CHOOSE?

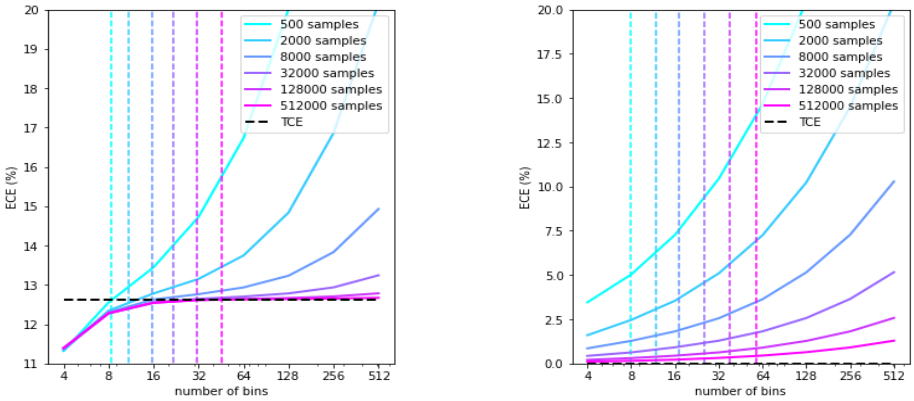

(a) Uncalibrated model.

(b) Perfectly calibrated model.

Figure 13: **Bins chosen by equal mass $\text{ECE}_{\text{SWEEP}}$ method**. We plot equal mass ECE_{BIN} % versus number of bins for various sample sizes n. We highlight the TCE with a horizontal dashed line and show the average number of bins chosen by the $\text{ECE}_{\text{SWEEP}}$ method for different sample sizes with vertical dashed lines. When the model is uncalibrated (left) $\text{ECE}_{\text{SWEEP}}$ chooses a bin number that is close to optimal. However, for perfectly calibrated models (right), the optimal number of bins is small (<=4), and $\text{ECE}_{\text{SWEEP}}$ does not do a good job of selecting a good bin number. The incorrect bin selection may partially explain why $\text{ECE}_{\text{SWEEP}}$ still has some bias for perfectly calibrated models. However, we note that any binning-based technique that always outputs a positive number will never be completely unbiased for perfectly calibrated models.

For Figure 13, the uncalibrated plot assumes $\mathbb{E}_Y[Y \mid f(X) = c] = \text{logistic}(10 * c - 5)$ while the calibrated plot assumes $\mathbb{E}_Y[Y \mid f(X) = c] = c$. Both experiments assume $f(x) \sim \text{Uniform}(0, 1)$.